Accurate Estimation without Calibration of the Complex Relative Permittivity of Multilayer Dielectric Material based on the Finite Integration Technique

Manh-Cuong Ho
Faculty of Electronics and Telecommunications, Electric Power University, Vietnam
cuonghm@epu.edu.vn

Trong-Hieu Le
Faculty of Electronics and Telecommunications, Electric Power University, Vietnam
hieult@epu.edu.vn (corresponding author)

Received: 7 February 2023 | Revised: 18 March 2023 | Accepted: 20 March 2023

Licensed under a CC-BY 4.0 license | Copyright (c) by the authors | *DOI: https://doi.org/10.48084/etasr.5665*

ABSTRACT

In this paper, a simple and effective solution is proposed to accurately estimate the complex relative permittivity of individual layers and multilayers of dielectric material samples from the S-parameters measured by two waveguide cells having equal or different lengths filled with the same vacuum/empty material without having to calibrate before performing experiments. The measurement system is set up by modeling using the Computer Simulation Technology (CST) software. In the modeling, a single layer/multilayer material sample is placed in the X-band rectangular waveguide and it has two ports used for the electromagnetic wave supply and measurement of S-parameters. From the S-parameters measured, the complex relative permittivity of individual layers and the multilayers of the material samples are estimated by the proposed method. The known single-layer and multilayer materials such as Garlock, Bakelite, and Teflon have different dielectric constants and thicknesses. The results show that the complex relative permittivity of the samples matches the measured and calculated values of S-parameters in the frequency range of 8.2GHz to 12.4GHz.

Keywords-complex relative permittivity; multilayer dielectric material; finite integration technique

I. INTRODUCTION

Multilayer dielectric material substrates are used in many practical applications, especially in high-speed circuits, such as the Microwave Integrated Circuits (MICs) [1, 2], Monolithic Microwave Integrated Circuits (MMIC) [3-6], and wireless systems applications [7, 8]. The exact knowledge of the individual layers in the multilayer substrate permittivity characterization is of great importance for MIC and MMIC design. The multilayer material is formed by composite materials and has new properties that could not be found in the individual layers. For the measurement of the electric properties over a wide frequency range, the waveguide method is one of the most popular methods to determine the permittivity of multilayer dielectric substrates [9-14]. In the waveguide measurement method, a sample of the composite multilayer substrate is placed in a waveguide and two port S-parameters are measured using a Vector Network Analyzer. This nondestructive method is based on the reflection coefficient and transmission coefficient measurement from which the complex permittivity (ε_r) or the permeability (μ_r) of the materials can be determined. In addition, the sample preparation requirements are minimal, and the electric properties can be measured over a wide frequency range. However, the waveguide method is the same as the free space or transmission line method, which are less accurate due to the unavoidable measurement errors. Although there are calibration standards, such as the Short-Open-Load-Through (SOLT) [15-20], the Through-Reflect-Line (TRL) [21-24], and the multiline TRL [25-28], that should be performed before the experiments, these methods experience their own respective defects, such as the requirement of multi-measurement cells, or the presence of the air gap effect.

This paper proposes a new approach to estimate the complex relative dielectric based on only one measurement of the S-parameters of the sample to eliminate the defects mentioned above by assuming the waveguide cell with the length l is determined to be filled with empty air inside ($\varepsilon_r \approx 1.0$-$j0.0$) as a layer of dielectric material. The proposed method can eliminate the air gap between the waveguide and the surface of the material sample because the air layer in the

waveguide reaching the surface of the sample is considered to be an air dielectric layer.

II. PROPOSED MODEL ANALYSIS

The proposed non-calibrated model to accurately estimate the complex relative permittivity of a multilayer dielectric material based on the finite integration technique is illustrated in Figure 1. In the proposed model, between the two waveguide cells, the dielectric material layers have thickness d with an empty air region with length l. The analytical electromagnetic method [11] is used to determine the S_{11} and S_{21} parameters of the multilayer dielectric material sample placed in the two ports of the rectangular waveguide as shown in Figure 1. In Figure 1, the two waveguide cells are filled with the same vacuum/empty material and are defined as layer#1 and layer#N with parameters (ε_{r0}, μ_{r0}), and the multilayer substrate consists of layer#2 to layer#N-1, where the mth layer has parameters (ε_{rm}, μ_{rm}), with N >=3. They are located between the transverse planes at $z = z_{n-1}$ and $z = z_n$.

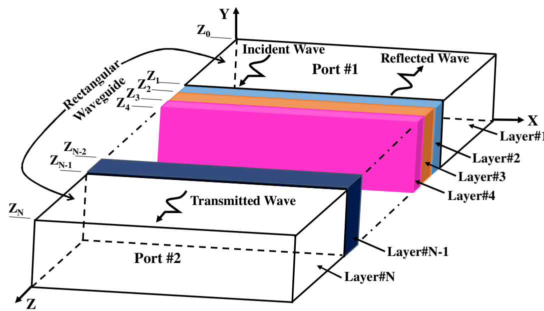

Fig. 1. Geometry of the multilayer dielectric material sample placed in the two ports of the rectangular waveguide for the estimation of S_{11} and S_{21}.

A. *Calculating Procedure of the S_{11} and S_{21} Parameters*

To determine the S_{11} and S_{21} components of 2-port parameters, it is assumed that the TE_{10} mode of unit amplitude is incident on the interface at $z = 0$ from the region $z \le 0$. If E_{t0}, E_{t1}, E_{t2}, ..., E_{tn} are the transverse electric fields on the interfaces at $z = z_0 = 0$, z_1, z_2, ..., z_n, respectively, then the transverse electric fields in the various regions of the waveguide are obtained as:

1) For $z \le 0$:

$$\vec{E}_0 = -2j\vec{e}_0 \sin(\beta_0^0 z) + \sum_{i=0}^{\infty}\left(\iint_{z=0} \vec{E}_{t0} * \vec{e}_i ds\right)\vec{e}_i e^{j\beta_i^0 z} \quad (1)$$

$$\vec{H}_0 = 2y_0^0\vec{h}_0 \cos(\beta_0^0 z) - \sum_{i=0}^{\infty}\left(\iint_{z=0} \vec{E}_{t0} * \vec{e}_i ds\right)y_i^0\vec{h}_i e^{j\beta_i^0 z} \quad (2)$$

2) For $z_{n-1} \le z \le z_n$:

$$\vec{E}_n = \sum_{i=0}^{\infty}\left(\frac{\vec{E}_{1n} + \vec{E}_{2n}}{\sin\left(\beta_i^n z_1\right)}\right)\vec{e}_i \quad (1)$$

where:

$$\vec{E}_{1n} = \sin\left(\beta_i^n\left(z_n - z\right)\right)\iint_{z=z_{n-1}} \vec{E}_{t(n-1)} * \vec{e}_i ds$$

$$\vec{E}_{2n} = \sin\left(\beta_i^n\left(z - z_{n-1}\right)\right)\iint_{z=z_n} \vec{E}_{tn} * \vec{e}_i ds$$

$$\vec{H}_n = \sum_{i=0}^{\infty}\left(\frac{\vec{H}_{1n} - \vec{H}_{2n}}{j\sin\left(\beta_i^n\Delta\right)}\right)y_i^n\vec{h}_i \quad (4)$$

where:

$$\vec{H}_{1n} = \cos\left(\beta_i^n\left(z_n - z\right)\right)\iint_{z=z_{n-1}} \vec{E}_{t(n-1)} * \vec{e}_i ds$$

$$\vec{H}_{2n} = \cos\left(\beta_i^n\left(z - z_{n-1}\right)\right)\iint_{z=z_n} \vec{E}_{tn} * \vec{e}_i ds$$

3) For $z \ge z_n$:

$$\vec{E}_{n+1} = \sum_{i=0}^{\infty}\left(\iint_{z=z_n} \vec{E}_{tn} * \vec{e}_i ds\right)\vec{e}_i e^{j\beta_i^{n+1}(z_n - z)} \quad (5)$$

$$\vec{H}_{n+1} = \sum_{i=0}^{\infty}\left(\iint_{z=z_n} \vec{E}_{tn} * \vec{e}_i ds\right)y_i^{n+1}\vec{h}_i e^{j\beta_i^{n+1}(z_n - z)} \quad (6)$$

4) For $z = 0$,

$$2y_0^0\vec{h}_0 = \sum_{i=0}^{\infty}\left[\left[y_i^0 + y_i^1\frac{\cos\left(\beta_i^1\Delta_1\right)}{j\sin\left(\beta_i^1\Delta_1\right)}\right]\iint_{z=z_{n-1}} \vec{E}_{t0} * \vec{e}_i ds\right]\vec{h}_i - \sum_{i=0}^{\infty}\left[\frac{y_i^1}{j\sin\left(\beta_i^1\Delta_1\right)}\iint_{z=z_n} \vec{E}_{t1} * \vec{e}_i ds\right]\vec{h}_i \quad (7)$$

5) For $z = z_n$:

$$0 = \sum_{i=0}^{\infty}\frac{y_i^n\vec{h}_i}{j\sin\left(\beta_i^n\Delta_n\right)}\iint_{z=z_{n-1}} \vec{E}_{t(n-1)} * \vec{e}_i ds + \sum_{i=0}^{\infty}\vec{h}_i\left(y_i^n\frac{\cos(\beta_i^n\Delta_n)}{j\sin\left(\beta_i^n\Delta_n\right)} + y_i^{n+1}\frac{\cos(\beta_i^{n+1}\Delta_{n+1})}{j\sin\left(\beta_i^{n+1}\Delta_{n+1}\right)}\right) \times \iint_{z=z_n} \vec{E}_{tn} * \vec{e}_i ds + \sum_{i=0}^{\infty}\frac{-y_i^{n+1}\vec{h}_i}{j\sin\left(\beta_i^{n+1}\Delta_{n+1}\right)}\iint_{z=z_{n+1}} \vec{E}_{t(n+1)} * \vec{e}_i ds \quad (8)$$

6) For the interface located at $z = z_N$:

$$0 = \sum_{i=0}^{\infty}\frac{y_i^N\vec{h}_i}{j\sin\left(\beta_i^N\Delta_N\right)}\iint_{z=z_{n-1}} \vec{E}_{t(N-1)} * \vec{e}_i ds + \sum_{i=0}^{\infty}\vec{h}_i\left(y_i^N\frac{\cos(\beta_i^N\Delta_N)}{j\sin\left(\beta_i^N\Delta_N\right)} + y_i^{N+1}\right) \times \iint_{z=z_n} \vec{E}_{tN} * \vec{e}_i ds \quad (9)$$

The obtained transverse electric fields over the interfaces are:

$$\vec{E}_{t0} = \sum_{j=0}^{j_0} T_{0j}\vec{e}_j, \vec{E}_{t1} = \sum_{J=0}^{J_1} T_{1J}\vec{e}_J,$$
$$\vec{E}_{tn} = \sum_{J=0}^{J_n} T_{nJ}\vec{e}_J, ...\vec{E}_{tN} = \sum_{J=0}^{J_N} T_{NJ}\vec{e}_J \quad (10)$$

where T_{0J}, T_{1J}, ..., T_{NJ} are the complex unknown coefficients. Using the Galerkin's procedure, the complex amplitudes T_{0J}, $J = 1, 2, 3, \ldots, J_0$, T_{1J}, $J = 1, 2, 3, \ldots, J_1$, T_{NJ}, $J = 1, 2, 3, \ldots, J_N$ are all zero due to the orthogonal nature of vector modal functions. The solution of $(N + 1)$ gives an estimate of the complex amplitudes T_{00}, T_{10}, T_{20}, T_{N0} from which S_{11} and S_{12} are determined as:

$$S_{11} = T_{00} - 1 \text{ and } S_{21} = T_{N0}e^{j\beta_0^0 z_N} \quad (11)$$

B. Calculation Procedure of S_{22} and S_{12} Parameters

The S_{22} and S_{12} parameters can be determined by following the procedure used for the estimation of S_{11} and S_{21}, and reverse the locations of the layers as illustrated in Figure 2.

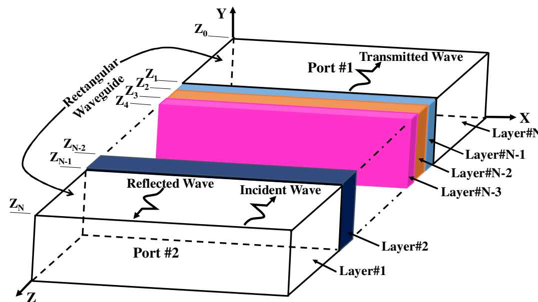

Fig. 2. Geometry of the multilayer dielectric material sample placed in the two ports of the rectangular waveguide for the estimation of S_{22} and S_{12}.

III. COMPLEX PERMITTIVITY ESTIMATION RESULTS

A. Estimation of S-Parameters

In this section, the properties of the individual layers of the dielectric material and of the empty layers are assumed to be known, the S-parameters for various material layers are computed from the theory as a functions frequency and are compared with the simulated S-parameters. The S-parameter simulations of both proposed models in Figures 1 and 2 were performed using the commercial 3-D full electromagnetic simulation software CST Microwave Studio. Figure 3 is based on the finite integration technique.

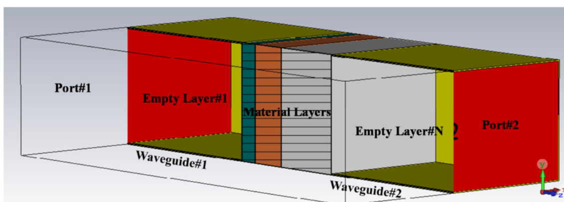

Fig. 3. Material layers with thickness d between two identical waveguide cells with an empty air region between them.

In Figure 3, the thickness d of the dielectric samples is assumed to be known, whereas the sample is placed between two identical waveguide cells with length l = 15mm and the empty air region with electric properties $\varepsilon_r = 1.0$.

B. Empty - Garlock - Empty

In this case, a single Garlock layer with thickness d = 1.7mm and $\varepsilon_r = 7.5 - j0.001$ is shown in Figure 4(a). The simulation results and the calculation of the S-parameters of the sample are shown in Figure 4(b)-(c). The results show that the simulated and calculated values of the S-parameters are almost similar in the frequency range from 8.2GHz to 12.4GHz.

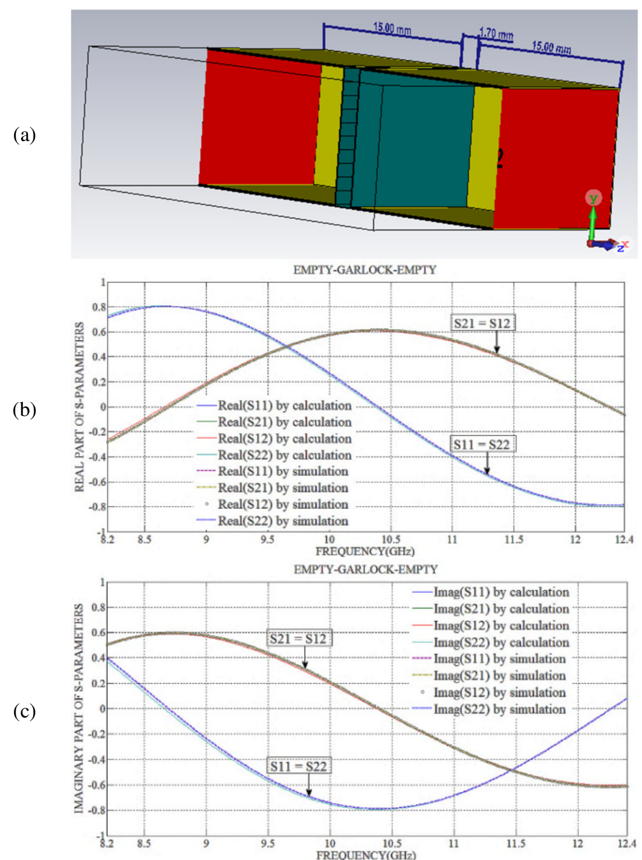

Fig. 4. (a) Garlock layer with d = 1.7mm between two identical waveguide cells with an empty air region between them with length l = 15mm, (b) real and (c) imaginary part of the simulated and calculated S-parameters of the Empty - Garlock - Empty layers.

C. Empty - Bakelite - Teflon - Empty

The considered composite sample consists of Bakelite and Teflon layers. The composite slab is formed by placing the Bakelite layer with d_1 = 3.3mm, $\varepsilon_r = 3.76 - j0.001$ and the Teflon layer with d_2 = 6.35mm, $\varepsilon_r = 2.03 - j0.001$ shown in Figure 5(a). The simulation and calculation results of the S-parameters of the sample are shown in Figure 5(b)-(c). The results show that the S-parameters simulated and calculated values agree well in the frequency range of 8.2GHz to 12.4GHz.

(a)

(b)

(c)

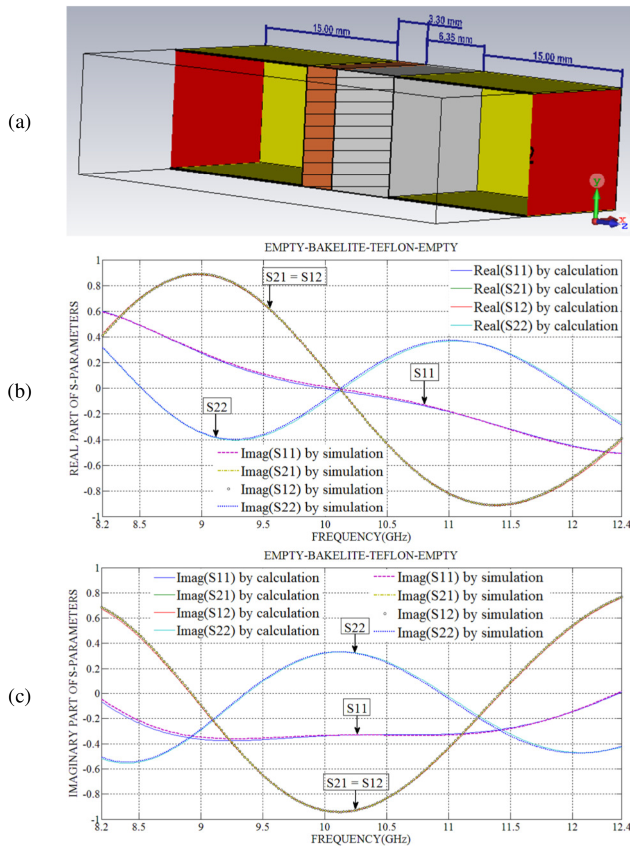

Fig. 5. (a) Bakelite and Teflon layers with thickness d_1 = 3.3mm and d_2 = 6.35mm between two identical waveguide cells with an empty air region of length l = 15mm, (b) real and (c) imaginary parts of the simulated and calculated S-parameters of Empty - Bakelite - Teflon - Empty dielectric layers.

D. Empty - Garlock - Bakelite - Teflon - Empty:

The composite sample considered consists of Garlock, Bakelite, and Teflon layers. The composite slab is formed by placing the Garlock layer with d_1 = 1.7mm, ε_r = 7.5 - j0.001, the Bakelite layer with d_2 = 3.3mm, ε_r = 3.76 - j0.001, and the Teflon layer with d_3 = 6.35mm, ε_r = 2.03 - j0.001 shown in Figure 6(a). The simulation and calculation results of the S-parameters of the sample are shown in Figure 6(b)-(c). The results show that the simulated and calculated values are in excellent agreement in the frequency range of 8.2GHz to 12.4GHz.

E. Estimation of Complex Permittivity

In this section, the simulated and calculated S-parameters of dielectric material samples, consisting of single or multilayer samples are used to estimate the complex permittivity based on the objective function and the MATLAB code from [11]. The results of the complex relative permittivity estimation of single-layer dielectric (Garlock), two-layer composite dielectric (Bakelite - Teflon), and three-layer composite dielectric (Garlock - Bakelite - Teflon) are shown in Figure 7, 8, and 9, respectively.

(a)

(b)

(c)

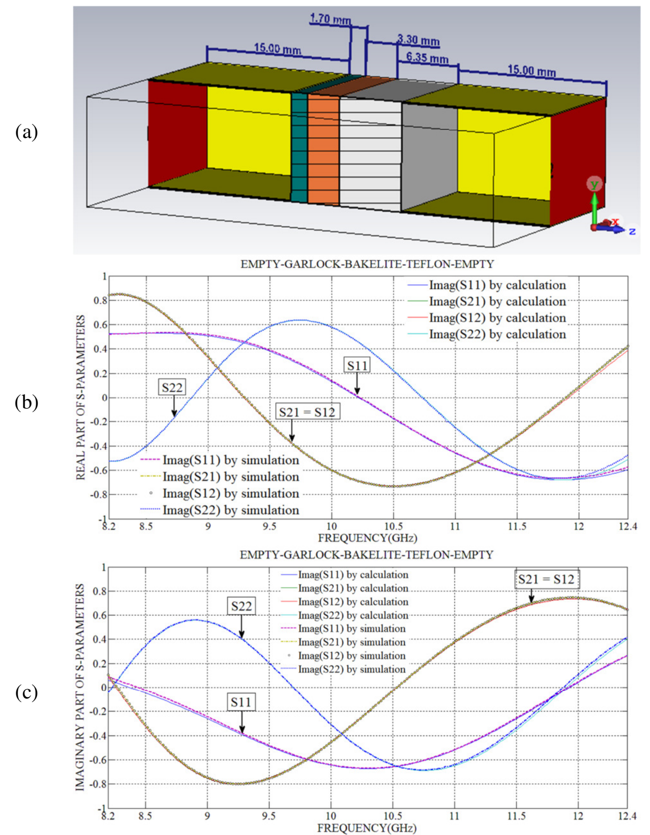

Fig. 6. (a) Garlock, Bakelite and Teflon layers with thickness d_1 = 1.7mm, d_2 = 3.3mmn and d_3 = 6.35mm between two identical waveguide cells with an empty air region with length l = 15mm, (b) real and parts of the simulated and calculated S-parameters of Empty - Garlock - Bakelite - Teflon - Empty dielectric layers.

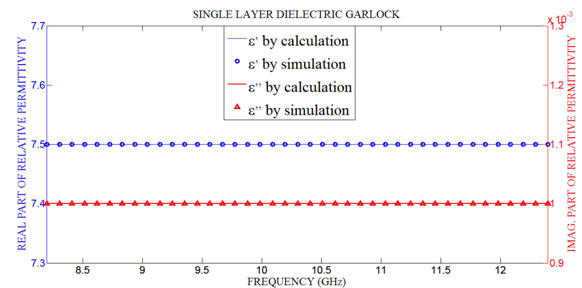

Fig. 7. Relative permittivity (real and imaginary) of Garlock material estimated using simulated and calculated S-parameters.

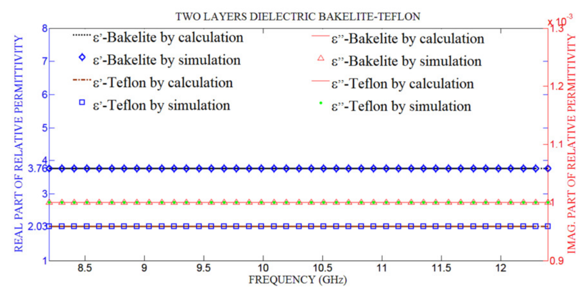

Fig. 8. Relative permittivity (real and imaginary) of Bakelite - Teflon material estimated using simulated and calculated S-parameters.

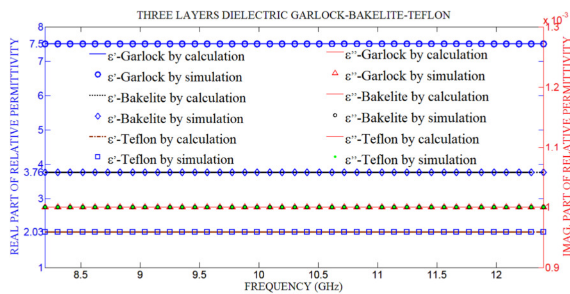

Fig. 9. Relative permittivity (real and imaginary) of Garlock - Bakelite - Teflon material estimated using simulated and calculated S-parameters.

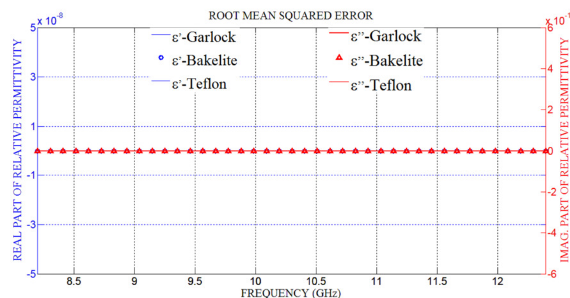

Fig. 10. The root mean square error of the complex relative permittivity between calculation and simulation.

The estimated results in Figures 7-10 show that that the error in the complex relative dielectric estimation from S-parameters simulated by the proposed waveguide calibration technique is extremely small or negligible in the frequency range of 8.2GHz to 12.4GHz.

IV. DISCUSSION

In this paper, a solution to eliminate the free space of the waveguide based on an improved measurement model and estimation algorithm is proposed. The novelty of the proposed model in comparison with the model in [11] is that there is no need to calibrate the waveguide when making the actual measurements because, in this study, the free space inside the waveguide is considered a layer of the dielectric material. However, the simulation test results show that the correctness of this solution is very satisfactory. In the future, we will continue to test this proposal by experimental measurements.

V. CONCLUSION

A simple and effective solution to estimate the complex relative permittivity of single and multi-layered dielectric material samples using waveguide measurements is proposed in this paper. The proposed system consists of modeling the S-parameters measurement using CST software combined with MATLAB. This estimation method is verified based on the complex relative permittivity estimation in the 8.2-12.4GHz frequency range of the reference composite samples Garlock, Bakelite, and Teflon, with known thicknesses. The results show that the simulated and ideal values of the complex relative permittivity of the samples presented an excellent agreement in the entire X-band without having to calibrate the waveguide cell before performing the experiments. The proposed method eliminates the effects of systematic errors of the calibrated experiment setup and thus can afford high measurement accuracy. Therefore, the proposed method is great for accurately estimating the complex relative permittivity of single- and multi-layered dielectric material samples.

ACKNOWLEDGMENT

This work was supported by the Faculty of Electronics and Telecommunications, Electric Power University (EPU), Hanoi, Vietnam.

REFERENCES

[1] L. Maloratsky, *Passive RF and Microwave Integrated Circuits*, 1st edition. Amsterdam, Netherlands: Newnes, 2003.

[2] I. Wolff, *Coplanar Microwave Integrated Circuits*. New York, NY, USA: John Wiley & Sons, 2006.

[3] S. Vinayak, H. P. Vyas, K. Muraleedharan, and V. D. Vankar, "Ni–Cr thin film resistor fabrication for GaAs monolithic microwave integrated circuits," *Thin Solid Films*, vol. 514, no. 1, pp. 52–57, Aug. 2006, https://doi.org/10.1016/j.tsf.2006.02.025.

[4] M. Garven and J. P. Calame, "Simulation and Optimization of Gate Temperatures in GaN-on-SiC Monolithic Microwave Integrated Circuits," *IEEE Transactions on Components and Packaging Technologies*, vol. 32, no. 1, pp. 63–72, Mar. 2009, https://doi.org/10.1109/TCAPT.2008.2004586.

[5] R. C. Fitch *et al.*, "Implementation of High-Power-Density X -Band AlGaN/GaN High Electron Mobility Transistors in a Millimeter-Wave Monolithic Microwave Integrated Circuit Process," *IEEE Electron Device Letters*, vol. 36, no. 10, pp. 1004–1007, Jul. 2015, https://doi.org/10.1109/LED.2015.2474265.

[6] M. Vellvehi, X. Perpina, J. Leon, O. Avino-Salvado, C. Ferrer, and X. Jorda, "Local Thermal Resistance Extraction in Monolithic Microwave Integrated Circuits," *IEEE Transactions on Industrial Electronics*, vol. 68, no. 12, pp. 12840–12849, Sep. 2021, https://doi.org/10.1109/TIE.2020.3040684.

[7] H. Alsaif, "Extreme Wide Band MIMO Antenna System for Fifth Generation Wireless Systems," *Engineering, Technology & Applied Science Research*, vol. 10, no. 2, pp. 5492–5495, Apr. 2020, https://doi.org/10.48084/etasr.3413.

[8] H. H. Alshortan, A. Alogla, M. a. H. Eleiwa, and M. I. Khan, "Low Cost High Gain 8×8 Planar Array Antenna for 5G Applications at 28GHz," *Engineering, Technology & Applied Science Research*, vol. 11, no. 6, pp. 7964–7967, Dec. 2021, https://doi.org/10.48084/etasr.4609.

[9] F. G. K. Abdulla and R. Abdulla, "A Comparative Application for Evaluating Composite Fabrics Used in Electromagnetic Shielding," *Engineering, Technology & Applied Science Research*, vol. 7, no. 6, pp. 2156–2159, Dec. 2017, https://doi.org/10.48084/etasr.1480.

[10] O. Tantot, M. Chatard-Moulin, and P. Guillon, "Measurement of complex permittivity and permeability and thickness of multilayered medium by an open-ended waveguide method," *IEEE Transactions on Instrumentation and Measurement*, vol. 46, no. 2, pp. 519–522, Apr. 1997, https://doi.org/10.1109/19.571900.

[11] M. D. Deshpande and K. Dudley, "Estimation of Complex Permittivity of Composite Multilayer Material at Microwave Frequency Using Waveguide Measurements," National Aeronautics and Space Administration, Washington, DC, USA, NAS 1.15:212398, May 2003.

[12] M. E. Baginski, D. L. Faircloth, and M. D. Deshpande, "Comparison of two optimization techniques for the estimation of complex permittivities of multilayered structures using waveguide measurements," *IEEE Transactions on Microwave Theory and Techniques*, vol. 53, no. 10, pp. 3251–3259, Jul. 2005, https://doi.org/10.1109/TMTT.2005.855133.

[13] D. L. Faircloth, M. E. Baginski, and S. M. Wentworth, "Complex permittivity and permeability extraction for multilayered samples using S-parameter waveguide measurements," *IEEE Transactions on Microwave Theory and Techniques*, vol. 54, no. 3, pp. 1201–1209, Mar. 2006, https://doi.org/10.1109/TMTT.2005.864104.

[14] F. Akleman, "Reconstruction of Complex Permittivity of a Longitudinally Inhomogeneous Material Loaded in a Rectangular Waveguide," *IEEE Microwave and Wireless Components Letters*, vol. 18, no. 3, pp. 158–160, Mar. 2008, https://doi.org/10.1109/LMWC.2008.916775.

[15] J. Stenarson and K. Yhland, "A new assessment method for the residual errors in SOLT and SOLR calibrated VNAs," in *69th ARFTG Conference*, Honolulu, HI, USA, Jun. 2007, pp. 1–6, https://doi.org/10.1109/ARFTG.2007.5456331.

[16] U. Stumper, "Influence of Nonideal Calibration Items on S-Parameter Uncertainties Applying the SOLR Calibration Method," *IEEE Transactions on Instrumentation and Measurement*, vol. 58, no. 4, pp. 1158–1163, Apr. 2009, https://doi.org/10.1109/TIM.2008.2006962.

[17] M. Schramm, M. Hrobak, J. Schur, and L.-P. Schmidt, "A SOLR calibration procedure for the 16-term error model," in *42nd European Microwave Conference*, Amsterdam, Netherlands, Nov. 2012, pp. 589–592, https://doi.org/10.23919/EuMC.2012.6459245.

[18] M. Seelmann-Eggebert *et al.*, "On the Accurate Measurement and Calibration of S-Parameters for Millimeter Wavelengths and Beyond," *IEEE Transactions on Microwave Theory and Techniques*, vol. 63, no. 7, pp. 2335–2342, Jul. 2015, https://doi.org/10.1109/TMTT.2015.2436919.

[19] C. Liu, A. Wu, C. Li, and N. Ridler, "A New SOLT Calibration Method for Leaky On-Wafer Measurements Using a 10-Term Error Model," *IEEE Transactions on Microwave Theory and Techniques*, vol. 66, no. 8, pp. 3894–3900, Dec. 2018, https://doi.org/10.1109/TMTT.2018.2832052.

[20] W. Zhao, C. Cheng, and L. Li, "Sensitivity Analysis of S-Parameter Measurements Due to Nonideal SOLR Calibration Standards," *IEEE Transactions on Instrumentation and Measurement*, vol. 70, pp. 1–10, 2021, https://doi.org/10.1109/TIM.2020.3038598.

[21] R. F. Kaiser and D. F. Williams, "Sources of Error in Coplanar-Waveguide TRL Calibrations," in *54th ARFTG Conference Digest*, Atlanta, GA, USA, Dec. 1999, vol. 36, pp. 1–6, https://doi.org/10.1109/ARFTG.1999.327367.

[22] U. Stumper, "Uncertainty of VNA S-parameter measurement due to nonideal TRL calibration items," *IEEE Transactions on Instrumentation and Measurement*, vol. 54, no. 2, pp. 676–679, Apr. 2005, https://doi.org/10.1109/TIM.2005.843521.

[23] R. K. Challa, D. Kajfez, V. Demir, J. R. Gladden, and A. Z. Elsherbeni, "Permittivity measurement with a non-standard waveguide by using TRL calibration and fractional linear data," *Progress In Electromagnetics Research B*, vol. 2, pp. 1–13, 2008, https://doi.org/10.2528/PIERB07102001.

[24] M. Potereau *et al.*, "Meander type transmission line design for on-wafer TRL calibration," in *46th European Microwave Conference*, London, UK, Oct. 2016, pp. 381–384, https://doi.org/10.1109/EuMC.2016.7824358.

[25] R. B. Marks, L. A. Hayden, J. A. Jargon, and F. Williams, "Time Domain Network Analysis using the Multiline TRL Calibration," in *44th ARFTG Conference Digest*, Boulder, CO, USA, Dec. 1994, vol. 26, pp. 47–55, https://doi.org/10.1109/ARFTG.1994.327080.

[26] D. F. Williams, C. M. Wang, and U. Arz, "An optimal multiline TRL calibration algorithm," in *MTT-S International Microwave Symposium Digest*, Philadelphia, PA, USA, Jun. 2003, vol. 3, pp. 1819–1822, https://doi.org/10.1109/MWSYM.2003.1210494.

[27] H. Lu, Z. Zhou, Chengwei, J. Zhou, T. Chen, and C. Chen, "A new on-wafer multiline thru-reflect-line (TRL) calibration standard design," in *3rd Asia-Pacific Conference on Antennas and Propagation*, Harbin, China, Jul. 2014, pp. 934–936, https://doi.org/10.1109/APCAP.2014.6992655.

[28] Y. Rolain, M. Ishteva, E. Van Nechel, and F. Ferranti, "A Tensor-Based Extension for the Multi-Line TRL Calibration," *IEEE Transactions on Microwave Theory and Techniques*, vol. 64, no. 7, pp. 2121–2128, Jul. 2016, https://doi.org/10.1109/TMTT.2016.2565474.